Supporting Information

Highly dispersed ultrafine Ru nanoparticles on the honeycomb-like N-doped carbon matrix with modified rectifying contact for enhanced electrochemical hydrogen evolution

Mingxin Pang,[+[a]] Yu Fang,[+[a]] Lizhang Chen,[[a]] Ruoxu Sun,[[a]] Xinyu Li,[[a]] Huan Pang,[[b]] Songtao Zhang,[[c]] Lin Xu,*[[a]] Dongmei Sun*[[a]] and Yawen Tang[[a]]

[a] Jiangsu Key Laboratory of New Power Batteries, Jiangsu Collaborative Innovation Center of Biomedical Functional Materials, School of Chemistry and Materials Science, Nanjing Normal University, Nanjing 210023, P. R. China

[b] School of Chemistry and Chemical Engineering, Yangzhou University, Yangzhou 225009, PR China

[c] Testing Center, Yangzhou University, Yangzhou 225009, PR China

[+] These authors contributed equally to this work.

Experimental Section

Reagents and chemicals

Sodium chloride (NaCl), gluconol ($C_6H_{12}O_6$), and hydroxylamine hydrochloride ($NH_2OH·HCl$) were supplied by Sinopharm Chemical Reagent Co., Ltd. Ruthenium (III) chloride trihydrate ($RuCl_3·xH_2O$) was provided by Shanghai Deb Biotechnology Co., LTD. Pt/C (20 wt.%) and RuO_2 were bought from Johnson Matthey Chemicals Co., Ltd. All of the chemical reagents were analytical grade and directly used as received without further purification.

Materials preparation

In a typical procedure, a solution including 6.5 mg of $RuCl_3·xH_2O$, 690 mg of $NH_2OH·HCl$ and 1 g of NaCl dissolved in 40 mL of deionized water was named as solution A. 500 mg of glucose powder was dissolved in 40 mL to form solution B. Then, solution A was added into solution B drop by drop under stirring, and the mixture was named as solution C. The precursors can be obtained by ultrasonic solution C for 1 h and dried under oven at 60 °C. Then, the recrystallized product prepared was transferred into a ceramic boat and then heated up to 800 ℃ with a ramp rate of 5 ℃·min^{-1} and maintained for 4 h under the flowing nitrogen atmosphere. Finally, the final Ru NPs@HNC product was obtained by washing with deionized water for several times and finally drying under a vacuum oven at 60 ℃.

For comparison, the HNC, Ru NPs@HC, and Ru NPs@NCNSs were also fabricated under the identical synthetic procedure except for the addition of $RuCl_3·xH_2O$, $NH_2OH·HCl$, and NaCl, respectively.

Materials characterization

X-ray diffraction (XRD) pattern was performed on a Rigaku D/max-RC diffractometer with a Cu Kα radiation (λ = 0.15406 nm). Scanning electron microscopy (SEM) measurement was carried out on a Hitachi S5500 scanning electron microscope. Transmission electron microscopy (TEM), high-resolution transmission electron microscopy (HRTEM), and energy-dispersive X-ray spectroscopy (EDX) mapping images were performed on a JEOL JEM-2010F TEM operated at an accelerating voltage of 200 kV. Raman test was conducted on a Raman spectrometer (Lab RAM HR800, λ = 514 nm). N_2 sorption measurement was investigated on a Micromeritics ASAP 2020 apparatus. X-ray photoelectron spectroscopy (XPS) and ultraviolet photoelectron spectroscopy (UPS) analyses were operated on a Thermo VG Scientific ESCALAB 250 spectrometer using Al Kα X-ray radiation and He I resonance lines (21.2 eV), respectively. Thermogravimetric analysis (TGA) was carried out on a Netzsch SSTA 449C thermal analyzer with a ramp rate of 10 °C min^{-1} under air atmosphere. Low-temperature N_2 adsorption measurements were performed using Micromeritics ASAP 2050 instrument.

Electrochemical Measurements

Electrochemical performances of electrocatalysts were evaluated by a three-electrode system connected with a DH7002A (Jiangsu Donghua Analytical Instrument CoLtd.) electrochemical workstation. A saturated calomel electrode (SCE), a carbon rod and a glassy carbon electrode (GCE) are served as the reference electrode, counter electrode and working electrode, respectively. The catalyst ink was prepared by

dispersing 5 mg of catalysts in 1.0 mL of ethanol solution (the volume ratio of water to ethanol is 3:1) by ultrasonication for 30 min. Then, 8 μL of the catalyst ink was dropped on the polished GCE surface. After that, 2 μL of Nafion (5 wt.%, Sigma-Aldrich) was loaded on the catalysts modified GCE surface and dried for next electrochemical test. All potentials were converted to a reversible hydrogen electrode (RHE) based on the following equation: $E_{RHE} = E_{SCE} + 0.0592\ pH + 0.242$. The hydrogen evolution reaction (HER) measurements were evaluated by linear sweep voltammetry (LSV) corrected against Ohmic potential drop (*iR*) losses in N_2-saturated 1.0 M KOH solution at scan rate of 5 mV s^{-1}. Double-layer capacitance (C_{dl}) was determined by a series of cyclic voltammetry (CV) tests within a potential range of 0.15-0.25 V *vs*. reversible hydrogen electrode (RHE) at different scan rates from 20 to 100 mV s^{-1} in 1.0 M KOH solution. The LSV curves for HER were obtained in the potential range of 1.0-1.9 V with a scan rate of 1 mV s^{-1}. Electrochemical impedance spectroscopy (EIS) measurements were measured at a frequency between 0.01 Hz and 10^5 Hz. The stability measurements were evaluated by continuous CV scanning 3000 cycles at a scan rate of 0.1 V s^{-1}.

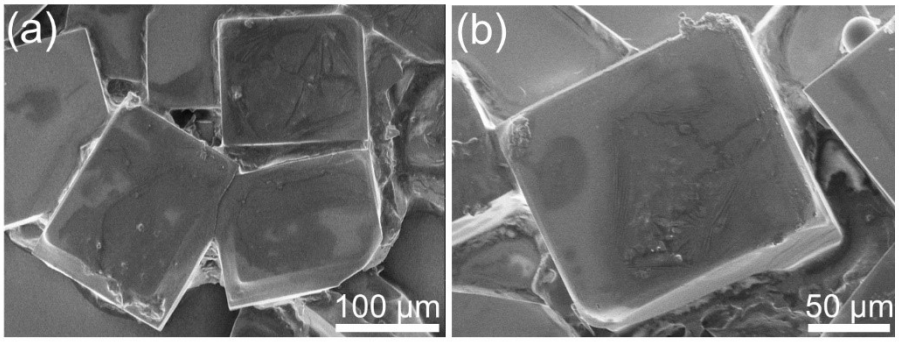

Figure S1. (a)-(b) SEM image of the formed $Ru^{3+}/C_6H_{12}O_6$@NaCl.

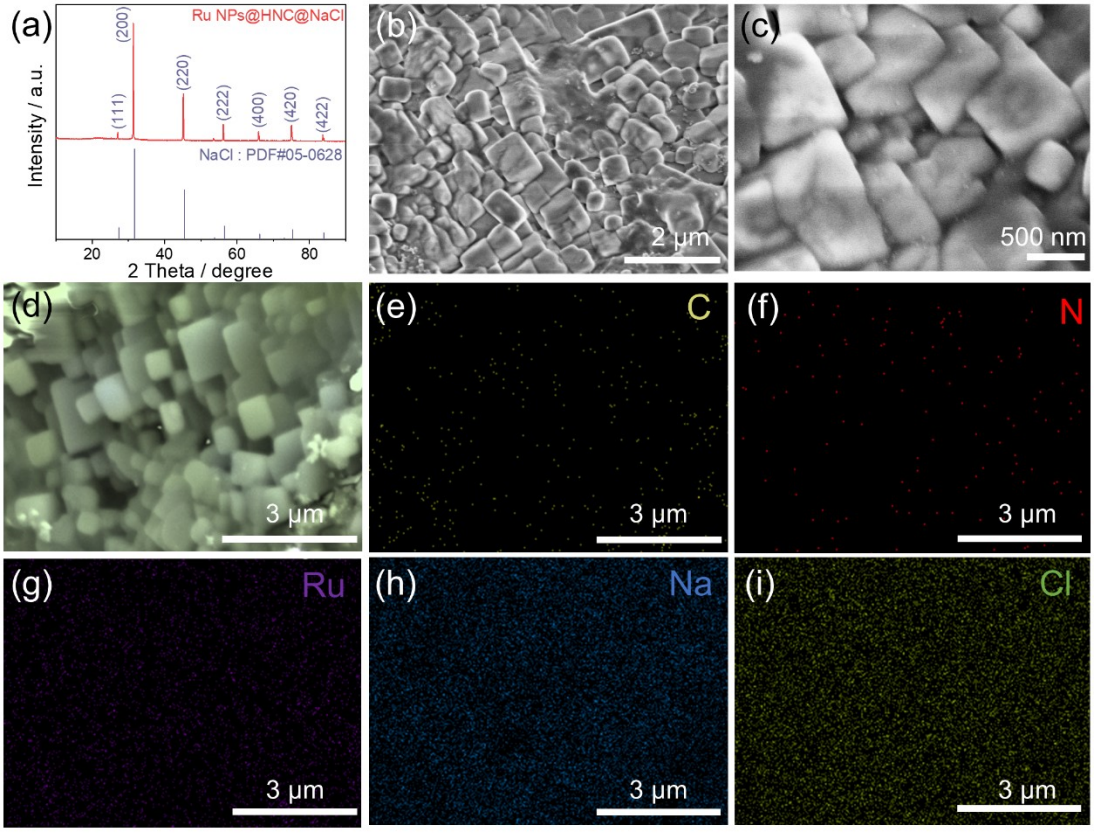

Figure S2 (a) XRD pattern, (b)-(c) SEM images and (d)-(i) elemental mapping images of the formed Ru NPs@HNC@NaCl.

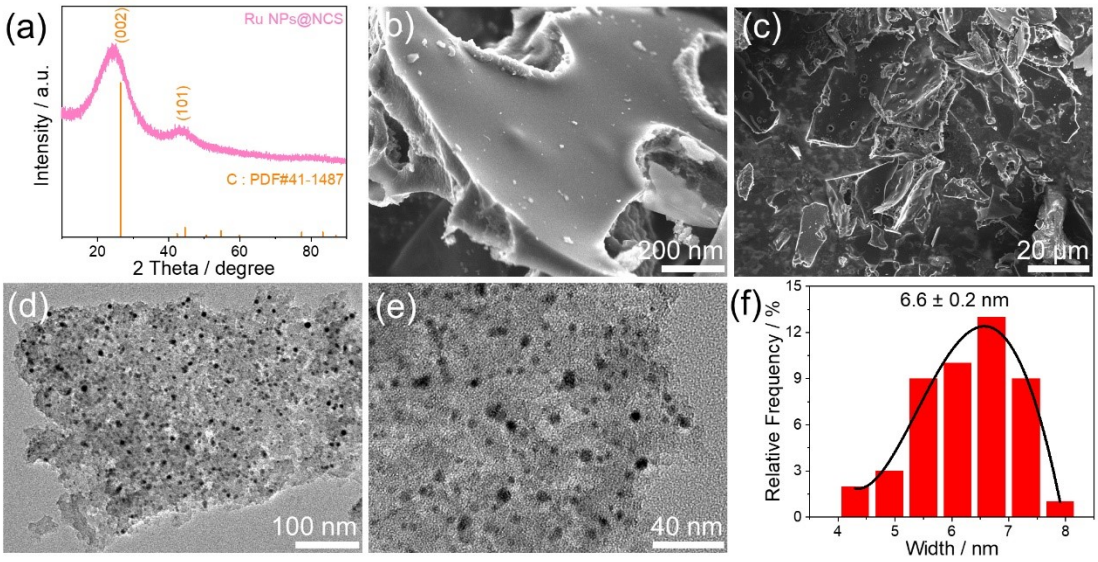

Figure S3. (a) XRD pattern, (b)-(c) SEM images, (d)-(e) TEM images and particle size distribution pattern of the formed Ru NPs@NCS.

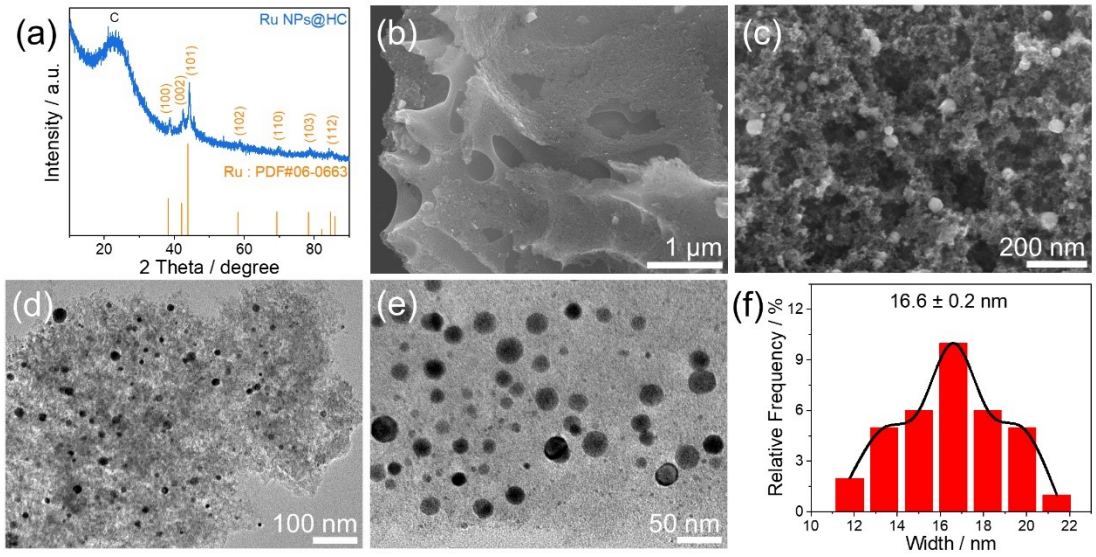

Figure S4. (a) XRD pattern, (b)-(c) SEM images, (d)-(e) TEM images and particle size distribution pattern of the formed Ru NPs@HC.

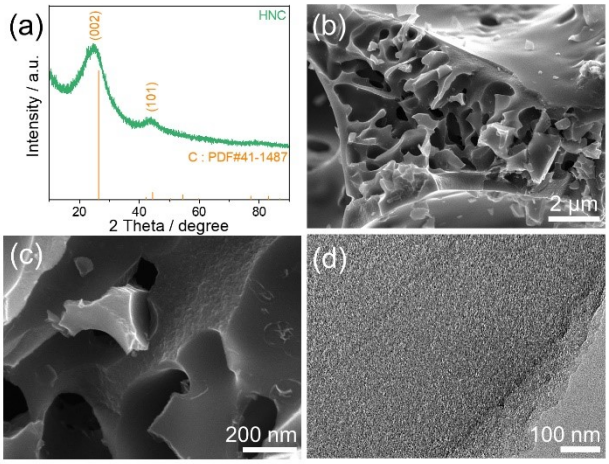

Figure S5 (a) XRD pattern, (b)-(c) SEM images, and (d) TEM image of the formed HNC.

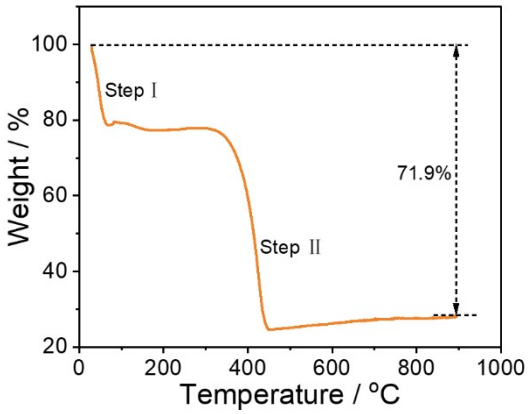

Figure S6 TGA curve of Ru NPs@HNC.

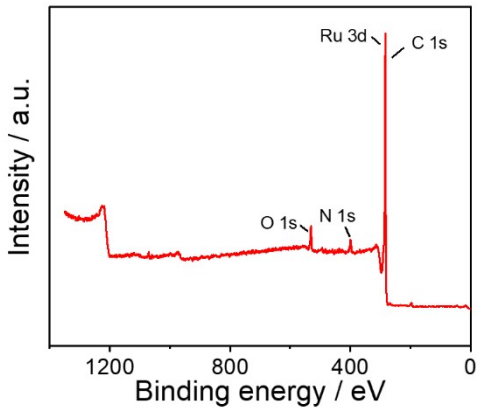

Figure S7 XPS survey scan spectrum of Ru NPs@HNC.

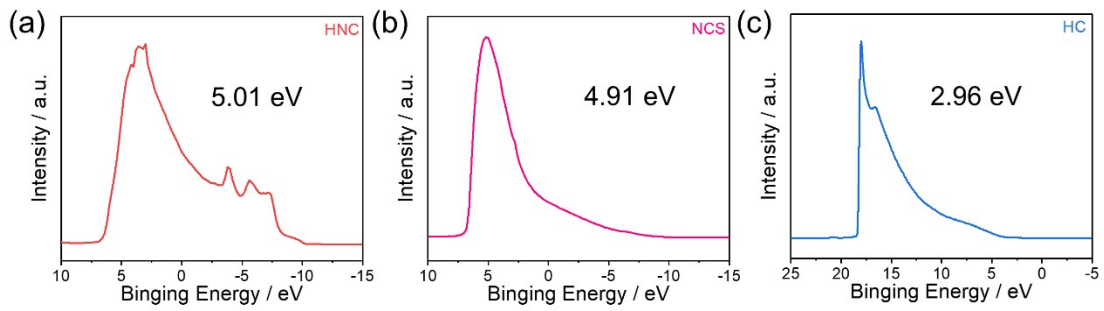

Figure S8 UPS spectra of pristine HNC, NCS and HC.

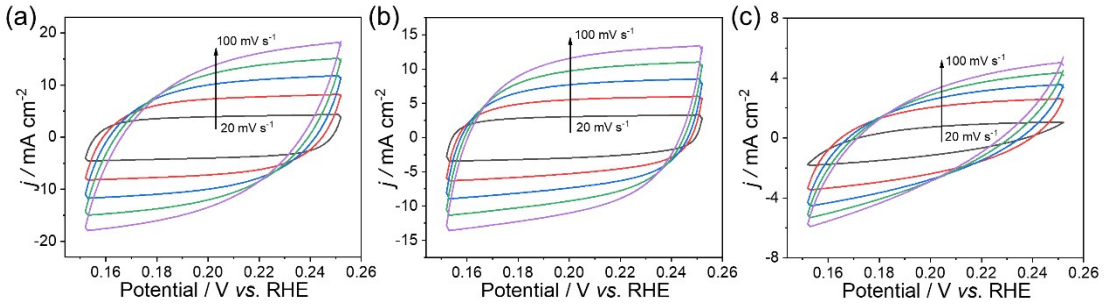

Figure S9. CV curves of (a) Ru NPs@HNC, (b) Ru NPs@HC, (c) Ru NPs@NCNSs in 1.0 M KOH at different scan rates of 20, 40, 60, 80, and 100 mV s^{-1}.

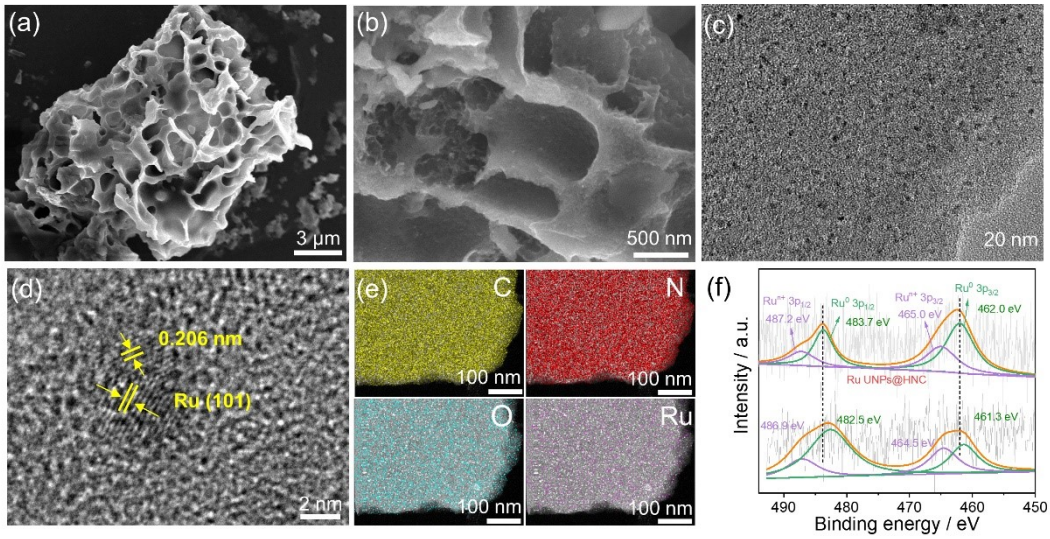

Figure S10. (a)-(b) SEM images, (c) TEM image, (d) HRTEM image and (e) elemental mapping images of Ru NPs@HNC after 3000 cycles CV test. (f) Ru 3p XPS spectra of Ru NPs@HNC before and after 3000 cycles CV test.

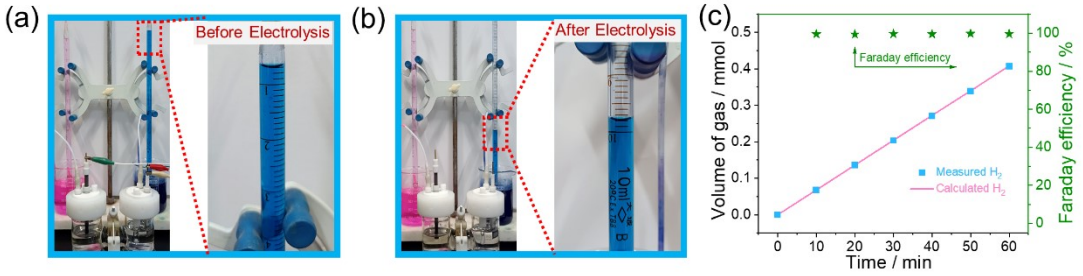

Figure S11 (a)-(b) Digital photographs of water splitting electrolyzer before and after the electrolysis. (c) Experimental and theoretical yields of H_2 gases during water splitting at a current density of 20 mA cm^{-2} and corresponding faradaic efficiency.

Table S1. The Ru content of Ru NPs@HNC measured by inductively coupled plasma atomic emission spectroscopy (ICP-AES).

Sample	wt.%
Ru NPs@HNC	2.19%

Table S2. The work functions of HNC, NCNSs, HC.

Sample	work function
HNC	5.01
NCNSs	4.91
HC	2.96

Table S3 Comparisons of HER activity of Ru NPs@HNC with some previously reported Ru-based catalysts in 1.0 M KOH solution.

Catalysts	η_j = 10 mA cm^{-2} /mV	Tafel slope /mV dec^{-1}	Reference
Ru NPs@HNC	**28**	**57.4**	**This work**
(Ru-Co)O_x/CC	44.1	23.5	*Angew. Chem. Int. Ed.*, 2020, 59, 17219.
Ru-NiCoP/NF	44	45.4	*Appl. Catal. B: Environ.*, 2020, 279, 119396.
Ru_1Ni_1-NCNFs	35	30	*Adv. Sci.*, 2020, 7, 1901833.
Sr_2RuO_4	61	51	*Nat. Commun.*, 2019, 10, 149.
Ru-MoS_2/CC	41	114	*Appl. Catal. B*, 2019, 249, 91-97.
Ru/NC-400	39	49	*Adv. Funct. Mater.*, 2021, 31, 2100698.
$Ru_{2.0}$/HNCS	72	67	*Mater. Today Phys.*, 2021, 16, 100300.
Ru_1CoP/CDs	51	73.4	*Angew. Chem. Int. Ed.*, 2021, 60, 7234.
Sr_2RuO_4	61	51	*Nat. Commun.*, 2019, 10, 149.
Ru-Ru_2P/PC-2	43.4	35.1	*J. Mater. Chem. A*, 2019, 7, 5621-5625.
RuP_2@NPC	52	69	*Angew. Chem. Int. Edit.*, 2017, 129, 11717-11722.
NiRu@NC	32	64	*J. Mater. Chem. A*, 2018, 6, 1376.
Ru/Co_4N-CoF_2	53	144.1	*Chem. Eur. J.*, 2021, 414, 128865.
Ru-Co_3O_4-NiO-NF	44	53.9	*Chem. Eur. J.*, 2021, 426, 131300.
M-Co NPs@Ru SAs/NC	34	55	*Small*, 2021, 17, 2105231.
Ru-NPs/SAs@N-TC	97	58	*Adv. Funct. Mater.*, 2020, 30, 2003007.
Ru/TiN-300	38	39	*Carbon Energy*, 2023, e391.
Ni_5P_4-Ru	54	52	*Adv. Mater.*, 2020,1906972.
Ru-MoS_2/CNT	50	62	*Adv. Sci.*, 2019, 6, 1900090.
Ru-$WO_{2.72}$	40	50	*Appl. Catal. B*, 2022, 308, 121229.

Table S4. Comparisons of overall water splitting performance of Ru NPs@HNC with those recently reported Ru-based electrocatalysts in 1.0 M KOH solution.

Catalysts	η_{10} (V vs. RHE)	Reference
Ru NPs@HNC	**1.557**	**This work**
Ru-SnS_2/CC-10	1.576	*Ind. Eng. Chem. Res.*, 2022, 61, 382.
Ru-FeRu@C/NC	1.63	*Chem. Eng. J.*, 2022, 437, 135456.
$Ru_{0.7}Co_{0.3}$ aerogel/CC	1.587	*J. Power Sources*, 2021, 514, 230600.
Ru_1Co_2 NPs	1.59	*ACS Appl. Energy Mater.*, 2020, 3, 1869.
Ru-Co_2P@Ru-N-C	1.56	*Adv. Funct. Mater.*, 2024, 2316709.
RuP/$CoNiP_4O_{12}$	1.56	*Appl. Catal. B* , 2023, 328, 122447.
（Ru-Co)O_x-350	1.57	*Chem. Eng. J.*, 2021, 420. 129805.
Ru-FeRu@C/NC	1.63	*Chem. Eng. J.*, 2022, 437, 135456.
Ru-H_2O/CC-350	1.67	*Appl. Catal. B*, 2022, 317, 121729.
Ru_1Ni_1-NCNFs	1.564	*Adv. Sci.*, 2020, 7, 1901833.
Ru-RuO_2/Mn-doped MoO_2	1.53	*Chem. Eng. J.*, 2023, 468, 143760.